

Article

# Synthesis and Encapsulation of a New Zinc Phthalocyanine Photosensitizer into Polymeric Nanoparticles to Enhance Cell Uptake and Phototoxicity

Nahid Mehraban <sup>1,\*</sup>, Phillip R. Musich <sup>2</sup> and Harold S. Freeman <sup>1,\*</sup><sup>1</sup> Fiber and Polymer Science program, North Carolina State University, Raleigh, NC 27606, USA<sup>2</sup> James H. Quillen College of Medicine, East Tennessee State University, Johnson City, TN 37684, USA; musichp@mail.etsu.edu

\* Correspondence: nahid.mehraban@gmail.com (N.M.); hfreeman@ncsu.edu (H.S.F.)

Received: 7 December 2018; Accepted: 22 January 2019; Published: 24 January 2019



**Abstract:** Efforts to enhance the utility of photodynamic therapy as a non-invasive method for treating certain cancers have often involved the design of dye sensitizers with increased singlet oxygen efficiency. More recently, however, sensitizers with greater selectivity for tumor cells than surrounding tissue have been targeted. The present study provides an approach to the modification of the known photosensitizer zinc phthalocyanine (ZnPc), to enhance its solubility and delivery to cancer cells. Targeting a photosensitizer to the site of action improves the efficacy of the sensitizer in photodynamic therapy. In this work we used PLGA-b-PEG to encapsulate a new zinc phthalocyanine derivative, 2(3), 9(10), 16(17), 23(24)-tetrakis-(4'-methyl-benzyloxy) phthalocyanine zinc(II) (ZnPcBCH<sub>3</sub>), to enhance uptake into A549 cells, a human lung cancer cell line. ZnPcBCH<sub>3</sub> exhibited the same photochemical properties as the parent compound ZnPc but gave increased solubility in organic solvents, which allowed for efficient encapsulation. In addition, the encapsulated dye showed a near 500-fold increase in phototoxicity for A549 cancer cells compared to free dye.

**Keywords:** PDT photosensitizer; phthalocyanine derivative; PLGA-b-PEG nanoparticles; phototoxicity

## 1. Introduction

Photodynamic therapy (PDT) is a noninvasive modality that can be used to treat cancers and certain oral and infectious diseases [1,2]. PDT involves the action of a photosensitizer (PS), oxygen, and light in combination to form reactive oxygen species (ROS) to kill cancer cells. In summary, upon absorption of a photon of light, a PDT sensitizer is promoted from the ground state ( $S_0$ ) to the short-lived first excited state ( $S_1$ ) and can undergo conversion to the first excited triplet state ( $T_1$ ) through intersystem crossing. Subsequently, the energy of the first triplet state can be transferred to the surrounding molecular oxygen ( $^3O_2$ ) to form a reactive species such as singlet oxygen ( $^1O_2$ ), and the sensitizer returns to  $S_0$ . This cycle can be repeated multiple times, depending on the photostability of the sensitizer. Studies have shown that the energy gap between  $T_1$  and  $S_0$  impacts the efficiency of the photosensitizer employed in PDT [3,4]. The higher the energy difference, the more efficient the energy transfer and the more efficient the sensitizer. The minimum energy difference ( $\Delta E_{S_0-T_1}$ ) needed between the two states in order for a fluorescent dye to function as a sensitizer ( $^1O_2$  producer) for PDT is 0.98 eV [5]. In this regard, molecular modeling tools can be used to screen potential photosensitizers for PDT use, by calculating  $\Delta E_{S_0-T_1}$ .

In addition to the efficiency of  $^1O_2$  production, other factors that may impact cellular-level PDT efficacy include: (1) biodistribution of the sensitizer employed, (2) subcellular localization of sensitizers

(i.e., to mitochondria or nuclei) [6,7], and (3) utilization of 100–200 nm nanoparticles to enhance photosensitizer delivery into cells. Nanoparticles within this size range are large enough to avoid rapid renal clearance and small enough to avoid removal by clearance via the reticuloendothelial system [6,8,9].

In the present work, zinc phthalocyanine (ZnPc) was chosen as the bench-mark sensitizer for our PDT studies. This dye–metal complex is from the porphyrin family, characterized by a hetero-aromatic system comprising 18  $\pi$  bonds. What makes this structure attractive for PDT is its good photostability and relatively long triplet-state lifetime [10]. The higher molar extinction coefficient of ZnPc compared to porphyrin dyes such as protoporphyrin IX is also attractive because it lowers both the dose level required for treatments and the associated side effects [11]. The main shortcoming of ZnPc is its low solubility in aqueous and organic solvents, which limits its utility for PDT. Generally, solubility limitations can also be overcome by the addition of suitable ligands in either of ZnPc's peripheral positions ( $\alpha$ ,  $\beta$ ; cf. Figure 1). It is known that the incorporation of alkyl groups can improve lipophilicity, which increases biological tissue distribution and volume of distribution. Incorporation of more or larger alkyl groups often reduces water solubility but occasionally this can increase water solubility through lowering the crystal lattice energy. Comparing branched vs. unbranched alkyl groups, the presence of multiple unbranched alkyl groups can lead to a large lipophilic surface area. Besides increasing the lipophilicity of ZnPc, it is also necessary for these compounds to have water solubility for the purpose of intravenous injection. Specifically, efforts have been made to improve water solubility of ZnPc compounds, through the introduction of hydrophilic groups such as  $-\text{CO}_2\text{H}$  and  $-\text{SO}_3\text{H}$ .

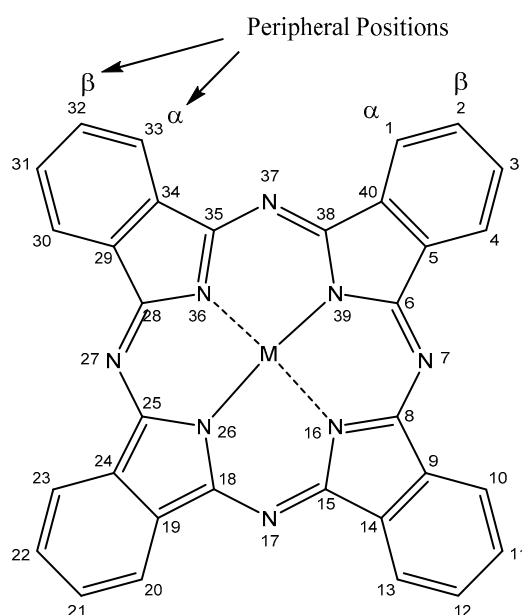


**Figure 1.** Common ( $\alpha$  and  $\beta$ ) vs. IUPAC systems for labeling metal (M) phthalocyanines.

Other attempts to overcome water insolubility have involved methods designed to encapsulate ZnPc into liposome or polymeric nanoparticles. In one study, ZnPc was encapsulated into poly(lactic-co-glycolic acid) (PLGA) nanoparticles having a diameter size of 227 to 450 nm utilizing the emulsion evaporation method [12]. Another research group attempted to encapsulate ZnPc into polycaprolactone (PCL) using a solvent emulsification-evaporation method to obtain nanoparticles with a diameter size of 187 nm [13]. However, neither of these previous studies reported on the cellular uptake of the particles obtained nor on the resultant cytotoxicity of the encapsulated dye.

It is known that the addition of substituents in the  $\alpha$  and  $\beta$  positions of ZnPc impacts the photophysical and photochemical properties of this system. Furthermore, new substituents can influence cell uptake and/or subcellular localization. Although hydrophobic (lipophilic) PSs have a

higher tendency to permeate cell membranes, their tendency to undergo aggregation in aqueous media makes them ineffective without a suitable delivery system. Hydrophobic PSs also tend to remain longer in the patient's body compared to hydrophilic PSs. These observations have caused PSs with amphiphilic properties through conjugation with water-soluble or amphiphilic polymers to become attractive in PDT studies [6,13–17].

While hydrophobic properties are essential to enhancing PS distribution in a tumor, water solubility is needed for intravenous administration and blood circulation of a PDT sensitizer. Adding a measure of water solubility can also be achieved by using biodegradable nanoparticles as a vehicle for delivery of the hydrophobic sensitizers to target cells. In addition to more effective transport of the sensitizer in serum and interstitial fluid, obtaining small nanoparticles should enhance passive permeation into encapsulated tumors to deliver the sensitizer to targeted cancer cells. Sensitizer encapsulation into nanoparticles also reduces the amount of dye needed for treatment, which subsequently reduces potential side effects. In addition, successful encapsulation will allow future modification of the nanoparticle surface to target specific cell types in order to reduce and/or prevent disease onset.

With the above points in mind, the goal of the present work was to enhance cellular uptake through modification of the ZnPc system and encapsulation of the resulting PS into nanoparticles. Specifically, *para*-methylbenzyloxy groups were added to ZnPc to form ZnPcBCH<sub>3</sub> and this dye was encapsulated into PLGA-b-PEG (Figure 2) nanoparticles. The choice of ZnPc analog was based on ease of synthesis and potential to enhance solvent solubility and potential to give suitable particle sizes following encapsulation. Following encapsulation, the photophysical and biological properties (cell uptake, dark and light toxicity) of free and encapsulated ZnPcBCH<sub>3</sub> were evaluated.

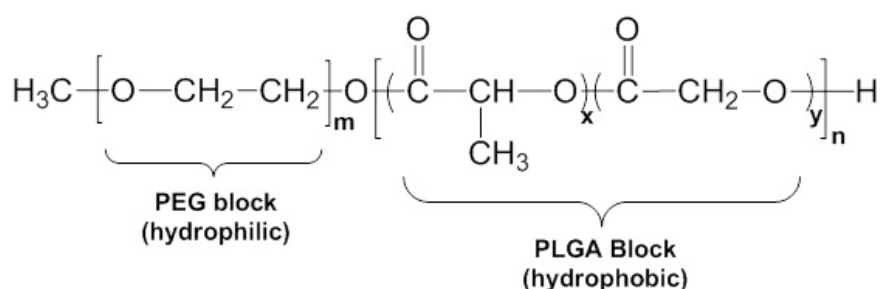


**Figure 2.** Structure of PLGA-b-PEG used for encapsulation of ZnPcBCH<sub>3</sub>, where n = 11,500, m = 2000, x = y.

## 2. Materials and Methods

**Chemicals:** Zinc phthalocyanine (ZnPc), 4-hydroxybenzoic acid, poly (ethylene glycol) methyl ether-block-poly (lactide-co-glycolide), known as PEG-b-PLGA, with PEG average  $M_m$  2000 and PLGA average  $M_n$  11,500 and 3-(4,5-dimethylthiazol-2-yl)-2,5-diphenyl-2H-tetrazolium bromide (MTT), and 1,8-diazabicycloundec-7-ene (DBU) were purchased from Sigma Aldrich (St. Louis, MO, USA). Dimethyl sulfoxide (DMSO) was purchased from Alfa Aesar (Haverhill, MA, USA), while dimethylformamide (DMF) and acetonitrile were purchased from Thermo Fisher Scientific (Raleigh, NC, USA).

**Biological Supplies:** Delbecco's Minimum Essential Media (DMEM)/High Glucose (SH30243.02) was purchased from Fisher Scientific. CellTiter-Blue<sup>®</sup> (CTB) cell viability assay reagent was purchased from Promega (Madison, WI, USA). NucBlue solution for staining nuclei in live cells was purchased from Thermo Fisher Scientific (Raleigh, NC, USA). Human A549 lung carcinoma cells were cultured in DMEM containing 10% v/v Fetal Bovine Serum (FBS). DMEM and Hyclone FBS were obtained from Thermo Fisher Scientific (Raleigh, NC, USA). Cells were incubated at 5% CO<sub>2</sub> at 37 °C. The phototoxicity of the encapsulated dye was evaluated using a Scope Light 2000-HORIBA and a 599 ± 50 nm long bandpass filter (Edmond Optics, Barrington, NJ, USA) was used.

**Instrumentation:**  $^1\text{H-NMR}$  spectra were recorded on a Varian 400 MHz spectrometer (Palo Alto, CA, USA), Fluorescence spectra were recorded on a Fluorolog-3 spectrofluorometer (HORIBA Jobin Yvon Inc., Clifton Park, NY, USA) and NanoLED-625 was used. FTIR spectra were recorded on a Nicolet Nexus 470 FTIR spectrophotometer (Thermo Fisher Scientific, Raleigh, NC, USA). UV-VIS measurements were recorded on a Cary 300 spectrophotometer (Agilent, Santa Clara, CA, USA). Plate readers were a Molecular Devices Spectramax Gemini XS fluorescence plate reader (Molecular Devices, San Jose, CA, USA) and a Molecular Devices SpectraMax UV/Visible spectrophotometric plate reader (San Jose, CA, USA). Singlet oxygen quantum yields were measured using an Edinburgh Analytical Instrument (FS920) and NIR PMT from HAMAMATSU (H10330A series): West Lothian, UK.

### 2.1. Dye Synthesis

The synthesis conducted was a modification of a method reported previously [18].

4-(4'-Methyl-benzyloxy)-phthalonitrile (**3**), 4-Nitrophthalonitrile (3 g, 17.34 mmol) and 4-methylbenzyl alcohol (2.12 g, 17.34 mmol) were dissolved in 20 mL of dry DMF and stirred under  $\text{N}_2$ . After 5 min,  $\text{K}_2\text{CO}_3$  (7.19 g, 52.01 mmol) was added and the reaction was stirred at 85 °C for 7 h. After cooling, the reaction mixture was poured into cold water. The crude product (1.75 g) was purified by column chromatography using silica gel (230–400 Mesh) and dichloromethane as the eluent, to give compound **3** (1.3 g, 30%) having  $R_f = 0.82$  and mp = 132–134 °C. FTIR ( $\text{cm}^{-1}$ ): 3044.9 (Ar-CH), 2949.5 (CH), 2235.3 (CN), 1600.3, 1560.0, 15175.5, 1487.3, 1470.0, 1428.9, 1382.5, 1355.4, 1301.6, 1279.9, 1251.7, 1210.9, 1200.4, 1183.9, 1172.5, 1091.1, 997.3, 965.2, 950.9, 920.2, 879.1, 859.0, 834.0, 819.2, 775.7.  $^1\text{H-NMR}$  (400 MHz,  $\text{DMSO-d}_6$ ):  $\delta$  8.02 (dd,  $J = 8.8$  Hz,  $J = 2.1$  Hz, 1H), 7.81 (t,  $J = 2.3$  Hz, 1H), 7.48 (dt,  $J = 8.8$  Hz,  $J = 2.5$  Hz, 1H), 7.35–7.27 (m, 2H), 7.18 (d,  $J = 6.6$  Hz, 2H), 5.19 (s, 2H), 2.28 (s, 3H). ESI-MS (Elemental composition  $\text{C}_{16}\text{H}_{12}\text{N}_2\text{O}$ ): Theoretical 271.08418  $[\text{M}+\text{Na}]^+$ ; Experimental 271.08381  $[\text{M}+\text{Na}]^+$ .

2(3), 9(10), 16(17), 23(24)-Tetrakis-(4'-methyl-benzyloxy) phthalocyanine zinc(II) (**4**), Compound **3** (174 mg, 0.7 mmol) was dissolved in 3 mL of dry DMF and 10 drops of DBU were added. While stirring the reaction under  $\text{N}_2$ ,  $\text{Zn}(\text{OAc})_2$  (38.4 mg, 0.175 mmol) was added and the mixture was heated to 150 °C and stirred for 18 h. After cooling, the solution was slowly added to cold water (50 mL). The solid was collected and washed with methanol until the solvent was colorless. The product was dried under vacuum at room temperature to give 149 mg, m.p. > 200 °C. FTIR ( $\text{cm}^{-1}$ ): 3044.9 (Ar-CH), 2922.9 (CH), 10607.6, 1516.9, 1487.7, 1455.8, 1397.2, 1377.1, 1338.1, 1277.1, 1223.7, 1180.2, 1119.2, 1093.4, 1050.1, 1019.4, 944.8, 802.4, 744.9, 744.9, 728.7.  $^1\text{H-NMR}$  (400 MHz,  $\text{DMSO}$ ):  $\delta$  ppm = 8.78 (dt,  $J = 26.5$  Hz,  $J = 8.0$  Hz, 2H), 8.52–8.31 (m, 2H), 7.73–7.47 (m, 12H), 7.46–7.17 (m, 12H), 5.47 (d,  $J = 9.8$  Hz, 8H), 2.41–2.27 (m, 12H).  $R_f = 0.87$  in 1:1 DCM/THF. HESI ( $\text{C}_{64}\text{H}_{48}\text{N}_8\text{O}_4\text{Zn}$ ): Theoretical 1057.31628  $[\text{M}+\text{H}]^+$ , Experimental  $[\text{M}+\text{H}]^+$  1057.31828. MS (MALDI):  $m/z$  1057.31828.

### 2.2. Singlet Oxygen Quantum Yield

Relative singlet oxygen quantum yield ( $\Phi_\Delta$ ) values were determined in DMF using ZnPc as a standard [19,20]. Solutions of ZnPc and ZnPcBCH<sub>3</sub> were prepared in DMF with a maximum absorbance of 0.1 to 0.2 at 699 nm and excited at 699 nm, where the excitation count for both standard and the sample are the same. The optical density (OD) of these samples at this wavelength and the area under the typical emission at 1270 nm were used to calculate singlet oxygen quantum yields using Equation (1):

$$\Phi_\Delta = \Phi_\Delta(\text{std}) \frac{A_{\text{obs}(x)} \cdot \text{OD}(\text{std})}{A_{\text{obs}(\text{std})} \cdot \text{OD}(x)}, \quad (1)$$

where  $\text{OD}(\text{std})$  and  $\text{OD}(x)$  are the absorbance of the ZnPc and ZnPcBCH<sub>3</sub>, respectively, at 699 nm.

A 625 nm band path filter was used to prevent mixing absorption or fluorescent emission with the emission at 1270 nm.

### 2.3. Relative Fluorescence Quantum Yield

Fluorescence quantum yield ( $\Phi_f$ ) measurements were conducted similar to the procedure described above for singlet oxygen measurements. ZnPcBCH<sub>3</sub> and ZnPc solutions were prepared in DMF within 0.09 to 0.1 absorbance units at 608 nm. The area of the fluorescence emission band and the recorded absorption spectra were used to calculate the fluorescence quantum yield using Equation (2). The conditions for the sample and standard were the same and this measurement was repeated twice on different days. ZnPc in DMF was used as a standard for the measurement ( $\Phi_f = 0.28$ ) [21]:

$$\Phi_f = \Phi_f(\text{std}) \frac{A_{\text{obs}(x)} \cdot OD(\text{std})}{A_{\text{obs}(\text{std})} \cdot OD(x)}, \quad (2)$$

where  $A(x)$  and  $A(\text{std})$  are areas under the fluorescence emission curves of the samples and the standard, respectively.  $OD(x)$  and  $OD(\text{std})$  are the optical density of the sample and standard, respectively.

### 2.4. Fluorescence Lifetime

Fluorescence lifetimes were measured using a time-correlated single photon counting method that was conducted on the ZnPc and ZnPcBCH<sub>3</sub> solutions in DMF. For these measurements, LUDOX solution was used as a prompt and it was excited at 625 nm using a NanoLED pulse laser. Measurements were repeated twice and performed at a repetition rate of 1 MHz and a band pass of 1.5 nm.

### 2.5. Polymeric Nanoparticle Preparation

Polymeric nanoparticles were prepared by modification of protocols obtained from the literature [22]. PLGA-b-PEG polymer (20 mg) was dissolved in 2 mL of tetrahydrofuran (THF), ZnPcBCH<sub>3</sub> (0.2 mg) was added and the mixture was stirred for 10 min. This mixture was added to sterile water dropwise, stirred uncovered for 2 h, and the THF was removed under a vacuum at RT. The resultant nanoparticles were collected by centrifugation at 12,000 G for 15 min and the pelleted nanoparticles were washed twice with sterilized water followed by centrifugation each time. The nanoparticles were suspended in sterile phosphate-buffered saline (PBS) for use in the cell uptake and cytotoxicity studies. To establish that changing organic solvents has no impact on PDI and nanoparticle size, the preparation of nanoparticles was repeated using acetone and acetonitrile instead of THF.

The nanoparticles prepared in THF were suspended in sterile phosphate buffered saline (PBS) for use in the cell uptake and cytotoxicity studies. The amount of ZnPcBCH<sub>3</sub> contained in 1  $\mu$ L of these nanoparticles in PBS is 7.9 pg.

### 2.6. TEM Measurement

The morphology of the nanoparticles was characterized using a JEOL 2010F Field Emission transmission electron microscope (TEM, Peabody, MA, USA): operating at 200 KV. Nanoparticle solutions in PBS were applied to carbon-coated grids, negatively staining with 1% phosphotungstate, and air-dried at room temperature before TEM examination.

### 2.7. Dynamic Light Scattering and Zeta Potential

The diameter, polydispersity index and zeta potential were measured using a Malvern Zetasizer S90 (Westborough, MA, USA). Samples were diluted in deionized water for this measurement without a stabilizer.

### 2.8. Sensitizer Load and Entrapment Efficiency

Loaded sensitizer concentration determinations were performed by preparing a standard curve of free ZnPc-BCH<sub>3</sub> and measuring the absorption in THF at 677 nm. To determine the amount of nanoparticles formed, fixed volumes of nanoparticle solution were lyophilized and the dry weight measured. Sensitizer encapsulation was measured by dissolving the lyophilized nanoparticles in THF and measuring the absorbance at 677 nm. Nanoparticle yield, sensitizer load and entrapment efficiency were calculated using standard equations (cf. Equations (3)–(5)) obtained from the literature [23].

$$\text{Nanoparticle yields (\%)} = \frac{\text{Weight of nanoparticles}}{\text{Weight of polymer and sensitizer fed initially}} \times 100\%. \quad (3)$$

$$\text{Sensitizer loading (\%)} = \frac{\text{weight of sensitizer in nanoparticles}}{\text{Weight of nanoparticles}} \times 100\% \quad (4)$$

$$\text{Entrapment Efficiency (\%)} = \frac{\text{Weight of the sensitizer in nanoparticle}}{\text{Weight of sensitizer fed initially}} \times 100\%. \quad (5)$$

### 2.9. Qualitative Analysis of Dye Lipophilicity

Solutions of ZnPc and ZnPcBCH<sub>3</sub> were prepared at 2 and 4 μM in DMSO, DMEM, and DMEM +10% FBS. The visible spectra of the resultant solutions were obtained using a plate reader.

### 2.10. Cellular Uptake and Subcellular Distribution of Free and Encapsulated Dyes in A549 Cells

A549 cells were seeded into a 96-well plate at a density of 7500 cells per well. Cells were treated with encapsulated nanoparticles when each well was 75–80% confluent. Cells in 100 μL of culture media were treated by the addition of 39.5, 79, 126.4 or 158 pg of ZnPc-BCH<sub>3</sub> encapsulated in nanoparticles (cf. Section 2.5) in triplicate, at incubation times of 2, 4, 6, and 15 h. To quantify the nanoparticle uptake, cells were washed with PBS and lysed by addition of 100 μL DMSO per well. Each plate was rocked at room temperature in subdued light for 10 min before fluorescence measurements. Lysed cells in DMSO were excited at 616 nm and fluorescence emission was recorded at 700 nm.

### 2.11. Dark and PDT Toxicity Assays

Cytotoxic effects of free ZnPc and ZnPcBCH<sub>3</sub>, and PLGA-b-PEG-encapsulated ZnPcBCH<sub>3</sub> on A549 cells were determined utilizing the CTB (CellTiter-Blue®) Assay, which is based on the ability of living cells to convert the redox dye resazurin to resorufin, a fluorescent compound. In this assay, a decrease in fluorescence intensity reflects a decrease in cell viability.

Herein, 7000 cells were seeded per well and incubated overnight. The cell media then was replaced with 100 μL of serum-free DMEM media and 2 μL (4 μM) of free ZnPc or ZnPcBCH<sub>3</sub> (0.08 μg dye) in DMSO or 20 μL of the nanoparticles (0.158 ng of ZnPcBCH<sub>3</sub> nanoparticles) in PBS was added to the designated wells to reach the total volume of 100 μL. Mock-treated cells received 2% of DMSO or 20 μL of PBS. These procedures were conducted in subdued light. After 24 h of incubation, 20 μL of CTB reagent was added to each well, to reach the total volume of 120 μL, and incubation continued for another 3 h. Fluorescence emission data were recorded at 590 nm after excitation at 560 nm.

To quantify PDT toxicity, the above CTB procedure was followed except that after 24 h of cell incubation with PS, media was removed and cells covered by 50 μL of PBS were exposed to 1.5 mW/cm<sup>2</sup> light for 4.5 min using a band path filter of 599 ± 50 nm. To express the light exposure toxicity, cells were incubated in complete media for another 24 h after exposure prior to addition of the CTB reagent.

### 2.12. Statistical Analysis

Experiments were repeated three times and a *P* value of 0.05 was accepted as a statistically significant difference between compared samples.

## 3. Results and Discussion

### 3.1. Synthesis

The synthesis of ZnPcBCH<sub>3</sub> (compound 4) was conducted in two steps (cf. Figure 3), beginning with the reaction between nitrophthalonitrile (compound 1) and benzyl alcohol (compound 2) in dry DMF to give the substituted benzylphenyl ether (compound 3). The target phthalocyanine (compound 4) was obtained by heating compound 3 in the presence of DBU and Zn(OAc)<sub>2</sub> in DMF under N<sub>2</sub>. Formation of compound 4 was confirmed using <sup>1</sup>H-NMR, in tandem with ESI and MALDI mass spectrometry.

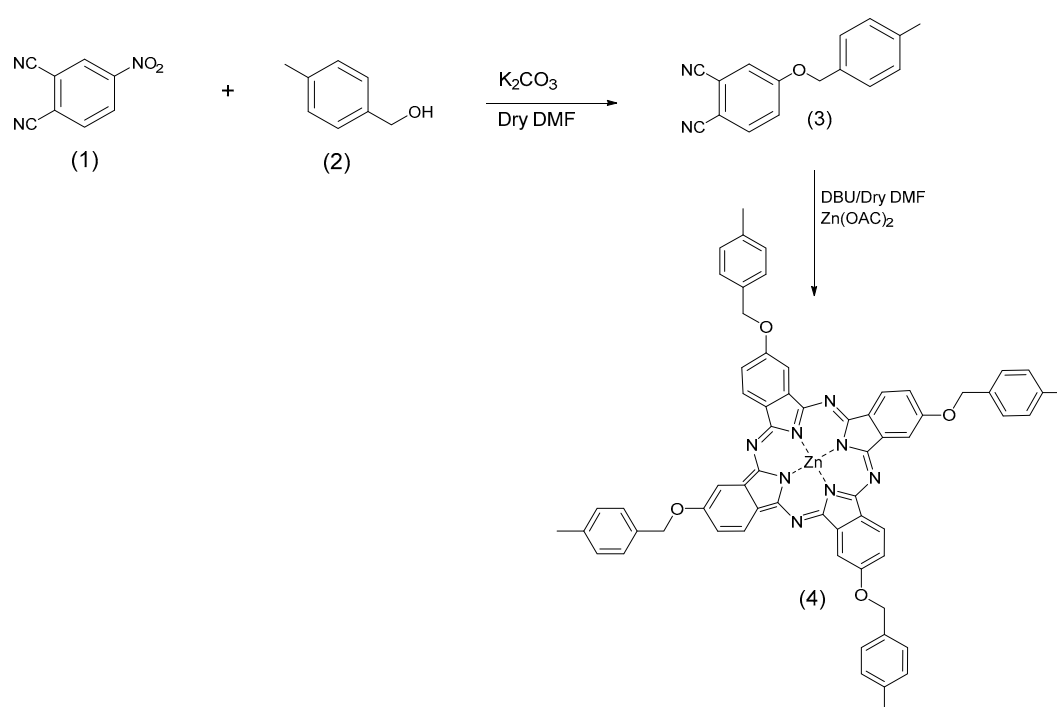


**Figure 3.** Two-step synthesis of the ZnPcBCH<sub>3</sub> sensitizer (4).

### 3.2. Photophysical and Photochemical Properties

The measured photophysical and photochemical properties of sensitizer (4) are summarized in Tables 1 and 2. Absorption and fluorescence emission spectra reflect a small bathochromic shift from replacing ZnPc with ZnPCBCH<sub>3</sub> (Figure 4). However, the significant increase (+480) in MW without altering the base chromogen caused a reduction in molar absorptivity ( $\epsilon$  value), as would be expected. No significant change was observed for decay lifetime ( $\tau_f$ ) when ZnPc ( $\tau_f$  3.166  $\pm$  0.002 ns) was converted to ZnPcBCH<sub>3</sub> ( $\tau_f$  3.132  $\pm$  0.002 ns). The molar extinction coefficient ( $\epsilon$ ) of ZnPc decreased from  $1.7 \times 10^5$  to  $1.6 \times 10^5$  for ZnPcBCH<sub>3</sub>, but the relative fluorescent quantum yield ( $\Phi_f$ ) increased significantly for ZnPc-BCH<sub>3</sub>. The higher fluorescence quantum yield for ZnPcBCH<sub>3</sub> compared to ZnPc indicates that intersystem crossing to the triplet state occurs less efficiently for ZnPcBCH<sub>3</sub>. This outcome is consistent with the decrease in <sup>1</sup>O<sub>2</sub> production ( $\Phi\Delta$ ) from ZnPcBCH<sub>3</sub>.

**Table 1.** Photophysical properties of ZnPc and ZnPcBCH<sub>3</sub> in DMSO obtained in plate reader with correction factor of 0.32.

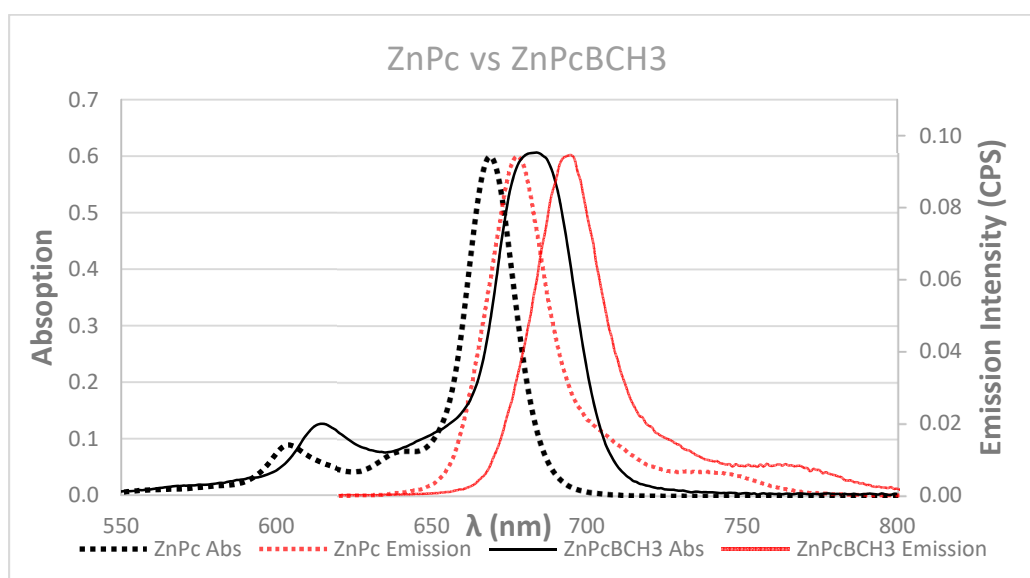
Compound	$\lambda_{ex}$ (nm) (Q) Band	$\epsilon$ (M <sup>-1</sup> cm <sup>-1</sup> )	$\lambda_{ex}$ (nm)	$\epsilon$ (M <sup>-1</sup> cm <sup>-1</sup> )	$\Phi_f$	$\tau_f$	$\Phi_\Delta$
ZnPc	672	$1.7 \times 10^5$	346	$8.58 \times 10^4$	$0.28 \pm 0.05$	$3.166 \times 10^{-9}$	$0.56 \pm 0.04$
ZnPcBCH <sub>3</sub>	677	$1.6 \times 10^5$	352	$6.4 \times 10^4$	$0.52 \pm 0.08$	$3.132 \times 10^{-9}$	$0.51 \pm 0.056$

$\epsilon$  (M<sup>-1</sup> cm<sup>-1</sup>) is molar extinction coefficient,  $\Phi_f$  is relative fluorescence quantum yield,  $\tau_f$  is the emission lifetime,  $\lambda_{ex}$  is the excitation lambda max, and  $\Phi_\Delta$  is singlet oxygen quantum yield.

**Table 2.** Absorption data recorded in DMF.

Compound	$\lambda_{abs}$ (DMF)	$\epsilon$ (M <sup>-1</sup> cm <sup>-1</sup> )	$\lambda_{Em}$	Stokes Shift
ZnPcBCH <sub>3</sub>	681 nm	$1.60 \times 10^5$	697 nm	16 nm
	612 nm	$3.41 \times 10^4$		

$\lambda_{abs}$  is the ground state excitation lambda max and  $\lambda_{Em}$  is the fluorescence emission lambda max.

**Figure 4.** Absorption and emission spectra of ZnPc and ZnPcBCH<sub>3</sub> in DMSO.

### 3.3. Characterization of Nanoparticles

To enhance the cell uptake and overcome the low water solubility of ZnPcBCH<sub>3</sub>, the sensitizer was encapsulated in PLGA-b-PEG polymeric nanoparticles using the nanoprecipitation method. The size and shape of the polymeric nanoparticles were determined using dynamic light scattering (DLS) and TEM, respectively (cf. Figure 5). Nanoprecipitation was carried out in different solvents to determine any change in size and zeta potential. The average diameter of polymeric nanoparticles was  $90.02 \pm 0.07$  nm using THF and  $97.82 \pm 0.01$  nm using acetone. Changing solvent for encapsulation did not have a significant impact on the polydispersity index (PDI) or the zeta potential of the nanoparticles (Table 3). These properties are in agreement with our reported zeta potential for the polymeric nanoparticles using THF or acetone ( $-9.74 \pm 0.01$  mV and  $-8.93 \pm 0.04$  mV, respectively). Representative TEM images showed that the formed nanoparticles from PLGA-b-PEG are spherical.

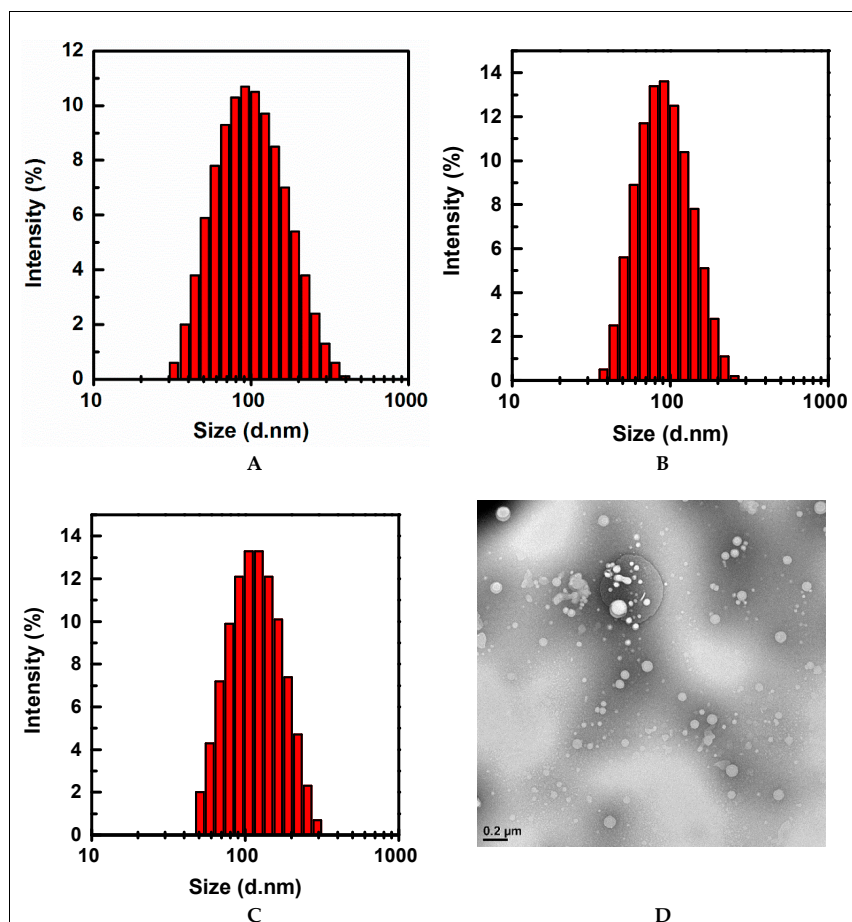


**Figure 5.** Diameter size distributions obtained from DLS for encapsulated ZnPcBCH<sub>3</sub> nanoparticles prepared in THF (A), acetone (B) and acetonitrile (C) media in the nanoprecipitation process, and TEM data for nanoparticles in acetonitrile (D).

**Table 3.** Characterization of PEG-b-PLGA nanoparticles formed in different solvents. Results represent mean  $\pm$  SD ( $n = 3$ ).

Particle Formation Solvent	Zeta Potential (mV)	Average Diameter (nm)	PDI
Acetone	$-8.93 \pm 0.04$	$97.82 \pm 0.02$	$0.209 \pm 0.003$
THF	$-9.74 \pm 0.01$	$90.09 \pm 0.10$	$0.202 \pm 0.003$
Acetonitrile	$-6.65 \pm 0.05$	$106.7 \pm 0.07$	$0.207 \pm 0.005$

As indicated in Table 3, regardless of the solvent choice, the zeta potential of the nanoparticles is  $\pm 10$  mV. This range of zeta potential indicates that the formed PLGA-b-PEG nanoparticle is a neutral particle [24] so that it interacts with cell membrane to facilitate the cell uptake. A PDI of less than 0.3 indicates a homogeneous particle distribution. Furthermore, the amount of encapsulated dye was measured using standard absorption curve for ZnPcBCH<sub>3</sub> in THF media, the results of which are summarized in Table 4.

**Table 4.** Nanoparticles yield, sensitizer load, and entrapment efficiency obtained from nanoprecipitation using THF.

Sample	ZnPcBCH <sub>3</sub>
Nanoparticle yield (%)	73.76
Dye sensitizer load (%)	0.37
Entrapment efficiency (%)	28

### 3.4. Lipophilicity of ZnPcBCH<sub>3</sub> and ZnPc

Lipophilicity was determined by measuring the absorbance of the two sensitizers in DMSO, DMEM, and DMEM + 10% FBS. The higher absorbance value for ZnPc in DMSO confirmed that the molar extinction coefficient of this dye is higher than for ZnPcBCH<sub>3</sub>, Table 1 and Figure 6. On the other hand, the higher absorption between 600–700 nm for ZnPcBCH<sub>3</sub> in DMEM + 10% FBS solution shows the higher interaction of this dye in FBS media compared to the ZnPc. The major protein in FBS is bovine serum albumin, which is known to contain hydrophobic pockets for binding lipids, fatty acids, and other non-polar components [25,26]. The higher absorbance observed for ZnPcBCH<sub>3</sub> compared to ZnPc in DMEM + 10% FBS (Figure 6) indicates the higher interaction of ZnPcBCH<sub>3</sub> with lipids and proteins in this cell culture media at the 2  $\mu$ M level. In support of the observed lipophilicity of ZnPcBCH<sub>3</sub> is the ability of ZnPcBCH<sub>3</sub> to dissolve in nonpolar organic solvents such as dichloromethane, while ZnPc does not.

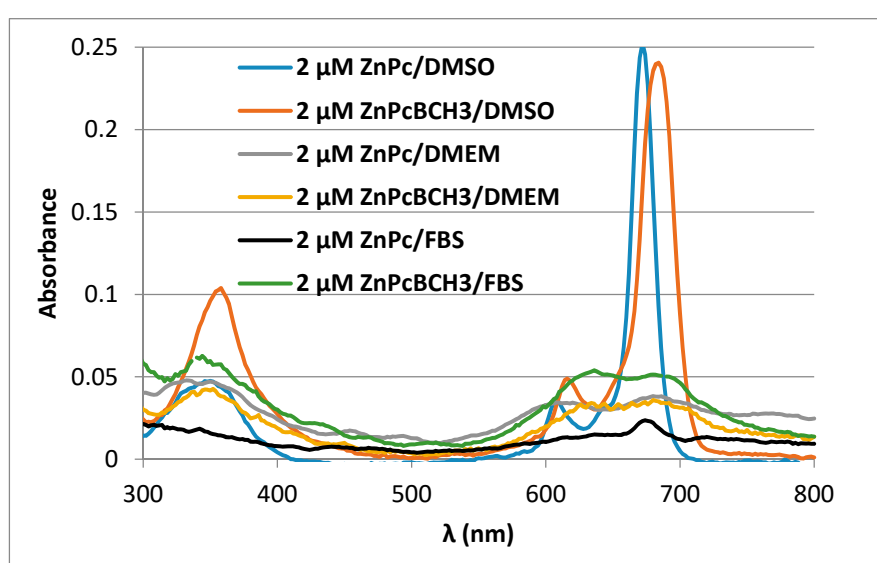


**Figure 6.** Monitoring the lipophilicity of ZnPc vs. ZnPcBCH<sub>3</sub> through the intensity of the visible spectra in DMSO, DMEM, and FBS media.

To increase the solubility of ZnPc in water or organic solvents, four benzyloxy groups with a small alkyl group were added to prepare ZnPcBCH<sub>3</sub>. This derivative dye exhibited high solubility in organic solvents such as THF, dichloromethane, and moderate solubility in acetone and acetonitrile. This suggests that increasing solubility in organic solvents results from increasing the lipophilicity of the parent dye. Bulky alkyl groups were not chosen since they would reduce rather than increase water solubility [27].

### 3.5. Localization of ZnPc and ZnPcBCH<sub>3</sub> in A549 Cells

To observe the subcellular localization of ZnPc and ZnPcBCH<sub>3</sub>, A549 cells were treated with 5  $\mu$ L of each dye sensitizer at 2  $\mu$ M concentration for 1 min. Cells were also treated with NucBlue to stain the DNA in the nucleus. The localization of ZnPc and ZnPcBCH<sub>3</sub> in A549 cells, shown in Figure 7, was monitored by fluorescence microscopy. The fluorescence associated with ZnPc appears green and the one for ZnPcBCH<sub>3</sub> appears red. Cell nuclei appeared as blue using NucBlue. These results show accumulation of the both ZnPc and ZnPcBCH<sub>3</sub> in the cytoplasm of A549 cells. In Figure 7, the images in the left column represent the location of ZnPc or ZnPcBCH<sub>3</sub>. Images in the middle column reveal the cell's nucleus stained with NucBlue. The right column shows the overlap of the first two images confirming the distinct cytoplasmic localization of ZnPc and ZnPcBCH<sub>3</sub>.

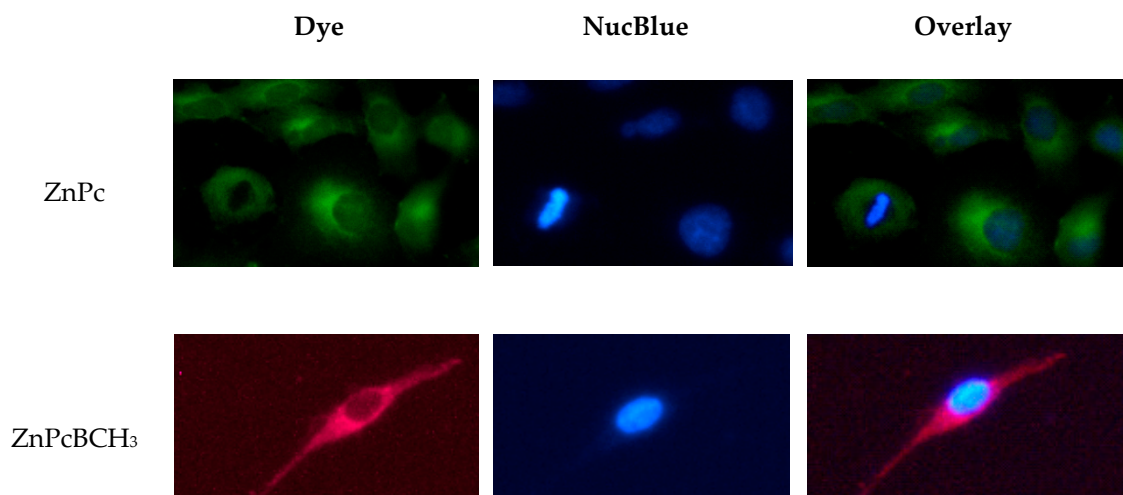


**Figure 7.** Subcellular distribution of ZnPC and ZnPcBCH<sub>3</sub> in A549 cells. After uptake the dyes were visualized using the Texas Red light cube for ZnPC, the Cy5 cube for ZnPc-BCH<sub>3</sub> and the DAPI cube for NucBlue.

### 3.6. Cell Uptake

One important aspect of a PDT study is to determine when to expose the cells to light following their treatment with the sensitizer. This is called the “optimized time” and occurs when dye uptake is maximized. Reaching the maximum uptake into cells is key to reaching the highest phototoxicity.

Cell uptake of the encapsulated nanoparticles of ZnPcBCH<sub>3</sub> was studied at different dye concentrations and incubation times. Figure 8 shows that increasing incubation time from 4 h to 15 h increased the amount of dye uptake. Also, a higher concentration of encapsulated dye resulted in higher cell uptake.

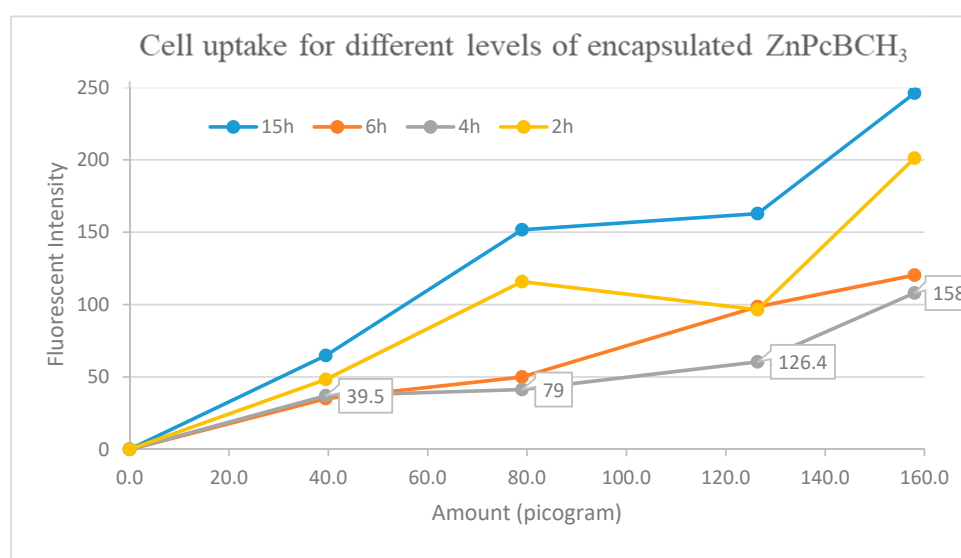


**Figure 8.** A549 cell uptake of encapsulated ZnPcBCH<sub>3</sub> at different incubation times and nanoparticle dye levels. The boxed numbers on the graph indicate the specific amounts of encapsulated ZnPcBCH<sub>3</sub> added. Higher fluorescence intensity (616<sub>Ex</sub>/700<sub>Em</sub>) indicates higher cell uptake of the encapsulated ZnPcBCH<sub>3</sub>.

### 3.7. Dye Toxicity

Dark toxicity of the ZnPC and ZnPcBCH<sub>3</sub> was assessed against A549 cells. The results, given in Figure 9, show that these dyes were nontoxic in the absence of light over 24 h (with *p* value > 0.05).

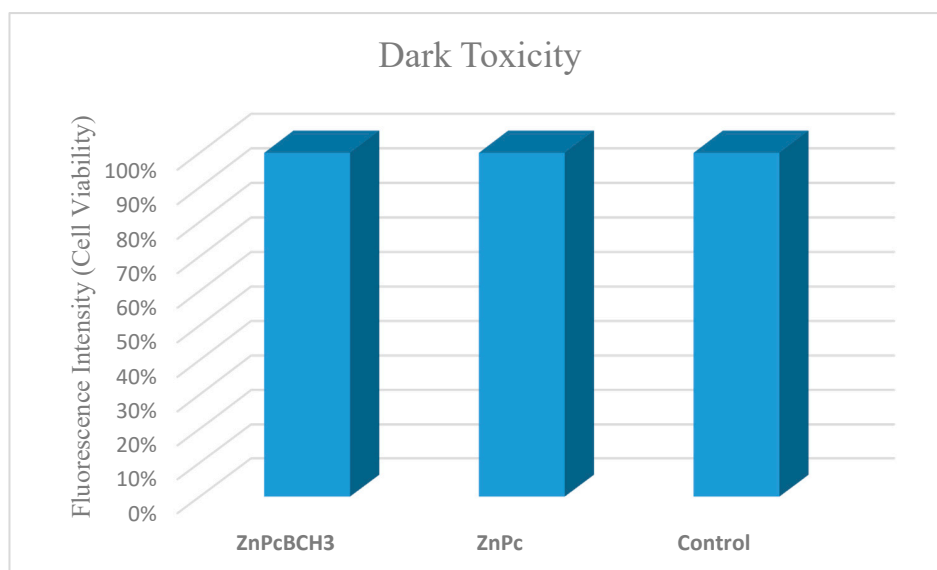


**Figure 9.** Dark toxicity results following a 24-h treatment of A549 cells with 80 nM ZnPc or ZnPcBCH<sub>3</sub> and 2% DMSO (control) using the CTB assay.

PDT cytotoxicity upon exposure to  $650 \pm 50$  nm light at  $1.5 \text{ mW/cm}^2$  revealed no significant cell killing for cells that were treated with free dyes, based on results from the CTB assay. However, the cell viability was significantly reduced for ZnPcBCH<sub>3</sub> encapsulated in a nanoparticle (Np) ( $p$  value = 0.003), with respect to the PBS control, empty nanoparticles, and free ZnPc-BCH<sub>3</sub> (Figure 10). Note that the actual ZnPcBCH<sub>3</sub> concentration was 500 times lower for cells receiving the nanoparticle treatment. Although the cytotoxicity of the encapsulated dye was significantly higher than the free dye, the cytotoxicity could be further enhanced by increasing the intensity and/or duration of the light exposure. The average size of mammalian cells is  $\sim 10\text{--}30 \mu\text{m}$  and subcellular organelles also can be larger than the nanoparticles. For example, mitochondria may be  $\sim 500 \text{ nm}$  [28]. Thus, further design and development of the nanoparticle to include mitochondrial targeting tags [29,30] in future work may improve the efficacy of the photosensitizer.

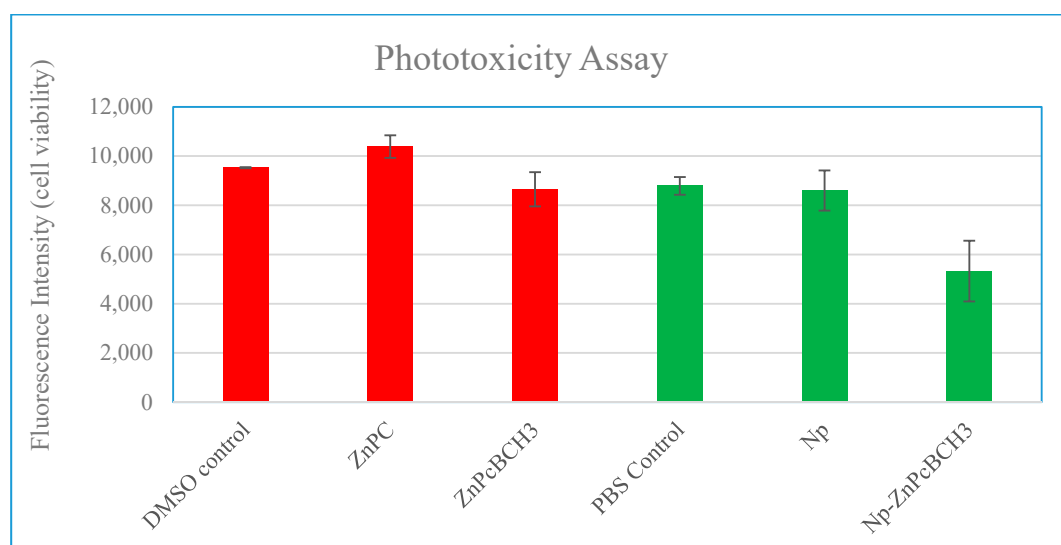


**Figure 10.** Phototoxicity of the encapsulated ZnPcBCH<sub>3</sub> vs free dyes. The A549 cells were exposed to 80 ng of ZnPc or ZnPcBCH<sub>3</sub> free dye versus 0.158 ng of ZnPcBCH<sub>3</sub> encapsulated into the PEG-b-PLGA nanoparticles. The viability of the A549 cells after dye treatment and light exposure was measured using the CTB assay.

#### 4. Conclusions

ZnPc can be modified to an analog (ZnPcBCH<sub>3</sub>) that is soluble in organic solvents and retains the desirable photochemical properties of ZnPc, by incorporating *para*-methylbenzyoxy groups in the  $\beta$ -positions of the ZnPc periphery. In addition, this modification allows for efficient encapsulation of ZnPcBCH<sub>3</sub> into PEG-b-PLGA nanoparticles, which affords a significant increase in A549 human cell uptake. The size and shape of the polymeric nanoparticles were readily determined using standard dynamic light scattering and transmission electron microscopy and the viability of the A549 cells after dye treatment and light exposure were measured using the CTB assay. The dark toxicity of the new analog remained low, while the light toxicity greatly increased about 500-fold. Although the cytotoxicity of the encapsulated dye is significantly higher than the free dye, it is anticipated that further enhanced cytotoxicity would be possible by increasing light exposure time/intensity.

**Author Contributions:** Conceptualization, N.M., P.R.M., H.S.F.; Methodology, N.M., P.R.M., H.S.F.; Validation, N.M., P.R.M., H.S.F.; Formal Analysis, N.M., P.R.M.; Investigation, N.M., P.R.M., H.S.F.; Resources, P.R.M., H.S.F.; Writing—Original Draft Preparation, N.M., P.R.M., H.S.F.; Writing—Review & Editing, N.M., P.R.M., H.S.F.; Supervision, P.R.M., H.S.F.; Project Administration, H.S.F.

**Funding:** Parts of this research were funded by East Tennessee State University's Research Development Committee grants numbered E82083 and E31231 (to P.R.M.).

**Acknowledgments:** The authors thank several colleagues at North Carolina State University for help with analytical measurements: Zhen Gu and Quanyin Hu (Department of Biomedical Engineering) and Ganesh Narayanan (Fiber and Polymer Science Program)—nanoparticle studies, Danielle Lehman (Department of Chemistry)—mass spectrometry studies, Arnab Chakraborty and Dr. Felix (Phil) Castellano (Department of Chemistry)—singlet oxygen studies.

**Conflicts of Interest:** The authors declare no conflict of interest.

#### References

1. Hamblin, M.R.; Hasan, T. Photodynamic therapy: A new antimicrobial approach to infectious disease? *Photochem. Photobiol. Sci.* **2004**, *3*, 436–450. [[CrossRef](#)] [[PubMed](#)]
2. Gursoy, H.; Ozcakir-Tomruk, C.; Tanalp, J.; Yilmaz, S. Photodynamic therapy in dentistry: A literature review. *Clin. Oral Investig.* **2013**, *17*, 1113–1125. [[CrossRef](#)]
3. Alberto, M.E.; De Simone, B.C.; Russo, N.; Sicilia, E.; Toscano, M. Can BODIPY Dimers Act as Photosensitizers in Photodynamic Therapy? A Theoretical Prediction. *Front. Phys.* **2018**, *6*, 143. [[CrossRef](#)]
4. Yogesh, G.; Nagaiyan, S. Investigating the excited state optical properties and origin of large Stokes shift in Benz[*c,d*]indole *N*-Heteroarene BF<sub>2</sub> dyes with ab initio tools. *J. Photochem. Photobiol. B Biol.* **2018**, *178*, 472–480.
5. Klán, P.; Wirz, J. *Photochemistry of Organic Compounds: From Concepts to Practice*; Wiley: Chichester, UK, 2009.
6. Mehraban, N.; Freeman, H.S. Developments in PDT sensitizers for increased selectivity and singlet oxygen production. *Materials* **2015**, *8*, 4421–4456. [[CrossRef](#)] [[PubMed](#)]
7. Rubio, N.; Fleury, S.P.; Redmond, R.W. Spatial and temporal dynamics of in vitro photodynamic cell killing: Extracellular hydrogen peroxide mediates neighbouring cell death. *Photochem. Photobiol. Sci.* **2009**, *8*, 457–464. [[CrossRef](#)]
8. Koo, H.; Lee, H.; Lee, S.; Min, K.H.; Kim, M.S.; Lee, D.S.; Choi, Y.; Kwon, I.C.; Kim, K.; Jeong, S.Y. In vivo tumor diagnosis and photodynamic therapy via tumoral pH-responsive polymeric micelles. *Chem. Commun.* **2010**, *46*, 5668–5670. [[CrossRef](#)]
9. Knop, K.; Mingotaud, A.; El-Akra, N.; Violleau, F.; Souchard, J. Monomeric pheophorbide (a)-containing poly(ethyleneglycol-*b*- $\epsilon$ -caprolactone) micelles for photodynamic therapy. *Photochem. Photobiol. Sci.* **2009**, *8*, 396–404. [[CrossRef](#)]
10. Rossetti, F.C.; Lopes, L.B.; Carollo, A.R.H.; Thomazini, J.A.; Tedesco, A.C.; Bentley, M.V.L.B. A delivery system to avoid self-aggregation and to improve in vitro and in vivo skin delivery of a phthalocyanine derivative used in the photodynamic therapy. *J. Control. Release* **2011**, *155*, 400–408. [[CrossRef](#)]
11. Fadel, M.; Kassab, K.; Fadeel, D.A. Zinc phthalocyanine-loaded PLGA biodegradable nanoparticles for photodynamic therapy in tumor-bearing mice. *Laser Med. Sci.* **2010**, *25*, 283–292. [[CrossRef](#)]

12. Da Volta Soares, M.; Mainara Rangel Oliveira, E.P.D.S.; de Brito Gitirana, L.; Barbosa, G.M.; Quaresma, C.H.; Ricci-Júnior, E. Nanostructured delivery system for zinc phthalocyanine: Preparation, characterization, and phototoxicity study against human lung adenocarcinoma A549 cells. *Int. J. Nanomed.* **2011**, *6*, 227–238.
13. Çakır, D.; Göksel, M.; Çakır, V.; Durmus, M.; Biyiklioglu, Z.; Kantekin, H. Amphiphilic zinc phthalocyanine photosensitizers: Synthesis, photophysical properties and in vitro studies for photodynamic therapy. *Dalton Trans.* **2015**, *44*, 9646–9658. [[CrossRef](#)] [[PubMed](#)]
14. Jin, H.; Zhang, X.; Zhang, B.; Kang, H.; Du, L.; Li, M. Nanostructures of an amphiphilic zinc phthalocyanine polymer conjugate for photodynamic therapy of psoriasis. *Colloids Surf. B* **2015**, *128*, 405–409. [[CrossRef](#)] [[PubMed](#)]
15. Doshi, M.; Krienke, M.; Khederzadeh, S.; Sanchez, H.; Copik, A.; Oyer, J.; Gesquiere, A.J. Conducting polymer nanoparticles for targeted cancer therapy. *RSC Adv.* **2015**, *5*, 37943–37956. [[CrossRef](#)]
16. Lo, P.C.; Huang, J.D.; Cheng, D.Y.Y.; Chan, E.Y.; Fong, W.P.; Ko, W.H.; Ng, D.K. New amphiphilic silicon (IV) phthalocyanines as efficient photosensitizers for photodynamic therapy: Synthesis, photophysical properties, and in vitro photodynamic activities. *Chem. Eur. J.* **2004**, *10*, 4831–4838. [[CrossRef](#)] [[PubMed](#)]
17. Theodossiou, T.A.; Gonçalves, A.R.; Yannakopoulou, K.; Skarpen, E.; Berg, K. Photochemical internalization of tamoxifens transported by a “Trojan-Horse” nanoconjugate into Breast-Cancer cell lines. *Angew. Chem. Int. Ed.* **2015**, *54*, 4885–4889. [[CrossRef](#)] [[PubMed](#)]
18. Karaođlan, G.K.; Gümrukçü, G.; Koca, A.; Gül, A.; Avciata, U. Synthesis and characterization of novel soluble phthalocyanines with fused conjugated unsaturated groups. *Dyes Pigm.* **2011**, *90*, 11–20. [[CrossRef](#)]
19. Tyson, D.S.; Henbest, K.B.; Bialecki, J.; Castellano, F.N. Excited state processes in ruthenium (II)/pyrenyl complexes displaying extended lifetimes. *J. Phys. Chem. A* **2001**, *105*, 8154–8161. [[CrossRef](#)]
20. Ogunsipe, A.; Maree, D.; Nyokong, T. Solvent effects on the photochemical and fluorescence properties of zinc phthalocyanine derivatives. *J. Mol. Struct.* **2003**, *650*, 131–140. [[CrossRef](#)]
21. Scalise, I.; Durantini, E.N. Synthesis, properties, and photodynamic inactivation of escherichia coli using a cationic and a noncharged zn (II) pyridyloxypthalocyanine derivatives. *Bioorg. Med. Chem.* **2005**, *13*, 3037–3045. [[CrossRef](#)]
22. Ferrari, M. Cancer nanotechnology: Opportunities and challenges. *Nat. Rev. Cancer* **2005**, *5*, 161–171. [[CrossRef](#)] [[PubMed](#)]
23. Papadimitriou, S.; Bikiaris, D. Novel self-assembled core-shell nanoparticles based on crystalline amorphous moieties of aliphatic copolyesters for efficient controlled drug release. *J. Control. Release* **2009**, *138*, 177–184. [[CrossRef](#)] [[PubMed](#)]
24. Clogston, J.D.; Patri, A.K. Zeta potential measurement. In *Characterization of Nanoparticles Intended for Drug Delivery*; McNeil, S., Ed.; Springer: Berlin/Heidelberg, Germany, 2011; pp. 63–70.
25. Hamilton, J.A.; Era, S.; Bhamidipati, S.P.; Reed, R.G. Locations of the three primary binding sites for long-chain fatty acids on bovine serum albumin. *Proc. Natl. Acad. Sci. USA* **1991**, *88*, 2051–2054. [[CrossRef](#)] [[PubMed](#)]
26. Majorek, K.A.; Porebski, P.J.; Dayal, A.; Majorek, K.A.; Porebski, P.J.; Dayal, A.; Zimmerman, M.D.; Jablonska, K.; Stewart, A.J.; Chruszcz, M.; Minor, W. Structural and immunologic characterization of bovine, horse, and rabbit serum albumins. *Mol. Immunol.* **2012**, *52*, 174–182. [[CrossRef](#)] [[PubMed](#)]
27. Dörwald, F.Z. *Lead Optimization for Medicinal Chemists: Pharmacokinetic Properties of Functional Groups and Organic Compounds*; Wiley-VCH: Weinheim, Germany, 2012.
28. Ezzeddine, R.; Al-Banaw, A.; Tovmasyan, A.; Craik, J.D.; Batinic-Haberle, I.; Benov, L.T. Effect of molecular characteristics on cellular uptake, subcellular localization, and phototoxicity of Zn(II) N-alkylpyridylporphyrins. *J. Biol. Chem.* **2013**, *288*, 36579–36588. [[CrossRef](#)]
29. Coulter, C.V.; Kelso, G.F.; Lin, T.K.; Smith, R.A.; Murphy, M.P. Mitochondrially targeted antioxidants and thiol reagents. *Free Radic. Biol. Med.* **2001**, *28*, 1547–1554. [[CrossRef](#)]
30. Kelso, G.F.; Porteous, C.M.; Coulter, C.V.; Hughes, G.; Porteous, W.K.; Ledgerwood, E.C.; Smith, R.A.; Murphy, M.P. Selective targeting of a redox-active ubiquinone to mitochondria within cells: Antioxidant and antiapoptotic properties. *J. Biol. Chem.* **2001**, *276*, 4588–4596. [[CrossRef](#)]

